Chapter 6

Measurements of the Strong Coupling Constant and the Colour Factors

Háblame toda la noche si me quieres convencer.
Un rato, una hora, un día. Un tiempo sin determinar.
Tarda una vida en contarme lo que me quieras contar.

In this chapter the measurements of the strong coupling constant, $\alpha_s(M_Z)$, from the four-jet rate, as well as the simultaneous measurement of the strong coupling constant and the colour factors are described. The structure of the chapter is as follows. First the α_s measurements from the four-jet rate are detailed. Three different methods have been employed giving results in perfect agreement among them, and with an important reduction in the total systematic error with respect to previous analyses based on two- and three-jet observables. Finally, the simultaneous measurement of the strong coupling and the colour factors is presented, with results in perfect agreement with previous ALEPH analyses and with a similar analysis from another LEP Collaboration, namely OPAL.

6.1 Measurements of the Strong Coupling Constant from the Four-Jet Rate

Many QCD studies have been carried out at LEP, in particular precise measurements of the strong coupling constant $\alpha_s(M_Z)$ [9]. For these measurements jet rates and so called event-shape variables have been used as they are very sensitive to the effects of gluon radiation, and usually defined such that the differential cross sections are directly

proportional to the strong coupling constant. The differential matrix elements in leading (LO) and next-to-leading order (NLO) for these two- and three-jet type quantities have been known for a long time [15], and for some of the variables even the resummation of large logarithms to all orders in perturbation theory has been carried out [45].

Some years ago, NLO corrections to infrared- and collinear-safe four-jet observables were computed [46, 47, 48, 50, 51, 52, 53, 24], which allow refined studies such as measurements of the strong coupling constant with variables for which the perturbative predictions start at $\mathcal{O}(\alpha_s^2)$.

In this section three α_s measurements are presented which use these new calculations. The resummed next-to-leading order predictions for the four-jet rate, corrected to detector level, are fitted to ALEPH data. The theoretical input as well as the analysis procedure have been described in Chapters 3 and 5, respectively. Here plots and details about the corrections, the fit range, systematic uncertainty studies and a discussion of the results are given.

6.1.1 Corrections for the Four-Jet Rate

Hadronization Corrections

The resummed theoretical NLO prediction as obtained from DEBRECEN should be corrected for hadronization effects. This, as explained in the previous chapter, is done by computing the ratio of the hadron and parton level distributions.

In Fig. 6.1 the bin-by-bin hadronization corrections calculated with the various models described in Section 5.3.1 are shown. The two parton shower models PYTHIA and HERWIG give very similar corrections, which differ appreciably from unity, by about 20%. The corrections obtained with the PYTHIA,ME and PYTHIA,Q_0 options typically differ more from unity and are quite different from the previous ones. The large discrepancies at the order of 10% can be traced back to large discrepancies in the four-jet rates at parton and at hadron level. The parton shower option, for y_{cut}=0.008, gives a four-jet rate of 8.2% (6.9%) at parton (hadron) level, whereas the matrix element option predicts 10.2% (7.7%).

New MC models where the matrix element approach is combined with a parton shower have been studied, but they have been shown not to be suitable for the description of the

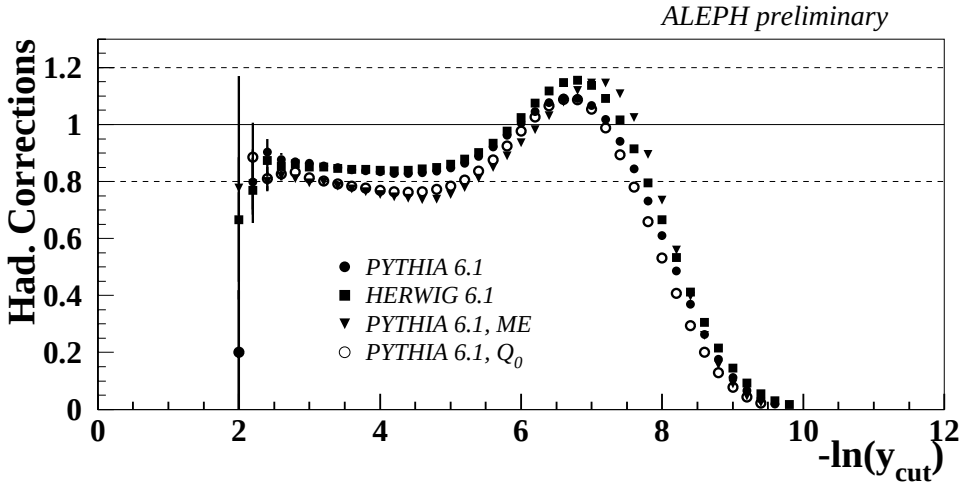

Figure 6.1: Comparison of the different hadronization corrections used in this thesis.

four-jet rate, as their predictions depend on an intrinsic resolution parameter needed to avoid soft and collinear divergences [43] (see also Chapter 7).

Detector Corrections

The theoretical prediction for the four-jet rate already corrected for hadronization effects, has to be corrected further to include detector effects before being compared to ALEPH data. As explained in the previous chapter, this is done by computing this observable from the MC before and after detector simulation.

The detector correction factors for the four-jet rate are typically found within the 5-10% range, increasing at the edges of the phase space. These corrections are displayed in Fig. 6.2.

Total Corrections

Taking into account the hadronization and detector corrections as explained above, the total corrections for the four-jet rate can be constructed as:

$$C^{\mathrm{tot}}(\mathrm{y_{cut}}) = C^{\mathrm{had}}(\mathrm{y_{cut}}) \cdot C^{\mathrm{det}}(\mathrm{y_{cut}}) \,. \tag{6.1}$$

Figure 6.3 shows the total bin-by-bin corrections. Typically they are about 10% in the central region of the four-jet rate, but quickly increasing to around 20% or higher when

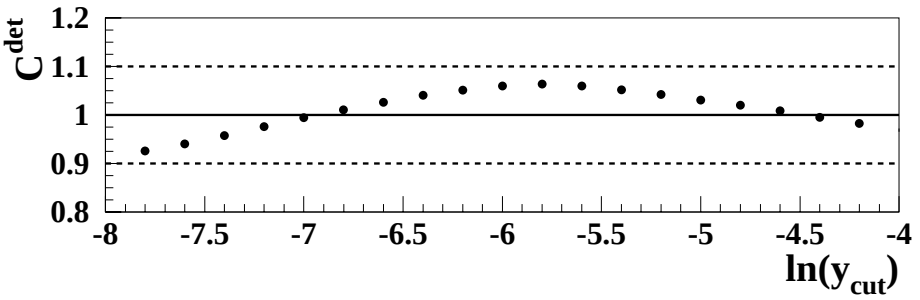

Figure 6.2: Detector corrections for the four-jet rate.

going to small or large y_{cut} values. Taking into account these total corrections, the fit range is selected by requiring them to be smaller than 10% and the resolution parameter to be in the range $10^{-3} < y_{cut} < 10^{-2}$.

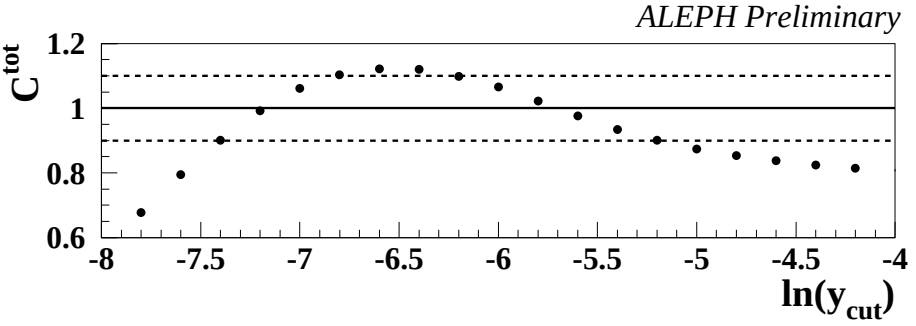

Figure 6.3: Total corrections for the four-jet rate. The dashed lines show the maximum allowed corrections used for the fit

6.1.2 Results

The experimental covariance matrix is calculated to take into account the statistical error of the data, the statistical errors of the detector and hadronization corrections, the statistical error of the theoretical prediction and the bin-by-bin statistical correlations among measurements of R_4 at different values of the resolution parameter. This covariance matrix is calculated following Eq. 5.12. Table 6.1 contains the four-jet rate from ALEPH data as well as the detector corrections. In Fig. 6.4 the correlations for the four-jet rate are plotted, showing values up to 90% for neighbouring y_{cut} values.

$\ln(y_{cut})$	R_4 from ALEPH data	Detector Corrections
-2.2	0.000019 ± 0.000003	0.7932 ± 0.1424
-2.4	0.000089 ± 0.000006	0.7307 ± 0.0481
-2.6	0.000315 ± 0.000012	0.8768 ± 0.0267
-2.8	0.000801 ± 0.000019	0.9054 ± 0.0164
-3.0	0.001699 ± 0.000027	0.9215 ± 0.0112
-3.2	0.003317 ± 0.000038	0.9276 ± 0.0082
-3.4	0.005744 ± 0.000050	0.9382 ± 0.0062
-3.6	0.009197 ± 0.000063	0.9494 ± 0.0050
-3.8	0.013923 ± 0.000078	0.9582 ± 0.0040
-4.0	0.020152 ± 0.000093	0.9683 ± 0.0034
-4.2	0.028218 ± 0.000110	0.9824 ± 0.0029
-4.4	0.038261 ± 0.000127	0.9945 ± 0.0025
-4.6	0.050409 ± 0.000145	1.0087 ± 0.0022
-4.8	0.064992 ± 0.000163	1.0197 ± 0.0019
-5.0	0.082198 ± 0.000182	1.0304 ± 0.0017
-5.2	0.102317 ± 0.000201	1.0422 ± 0.0015
-5.4	0.125528 ± 0.000220	1.0518 ± 0.0014
-5.6	0.151787 ± 0.000238	1.0597 ± 0.0012
-5.8	0.180738 ± 0.000255	1.0632 ± 0.0011
-6.0	0.210446 ± 0.000270	1.0596 ± 0.0010
-6.2	0.239597 ± 0.000283	1.0505 ± 0.0009
-6.4	0.265663 ± 0.000293	1.0401 ± 0.0008
-6.6	0.285690 ± 0.000299	1.0260 ± 0.0008
-6.8	0.297560 ± 0.000303	1.0100 ± 0.0007
-7.0	0.298678 ± 0.000303	0.9937 ± 0.0007
-7.2	0.287528 ± 0.000300	0.9753 ± 0.0007
-7.4	0.265248 ± 0.000293	0.9572 ± 0.0008
-7.6	0.234053 ± 0.000281	0.9405 ± 0.0008
-7.8	0.196958 ± 0.000264	0.9255 ± 0.0009
-8.0	0.157385 ± 0.000241	0.9134 ± 0.0010

Table 6.1: Four-jet rate measurements at different values of y_{cut} from ALEPH data. The detector corrections are also given. Bins from -0.2 to -2.0 are not in the table because no event was found to be a four-jet event for those values of y_{cut}.

Then a χ^2 is constructed according to Eq. 5.13, where i and j run over the bins allowed by the fit range requirements. Three different minimizations of this χ^2 are carried out,

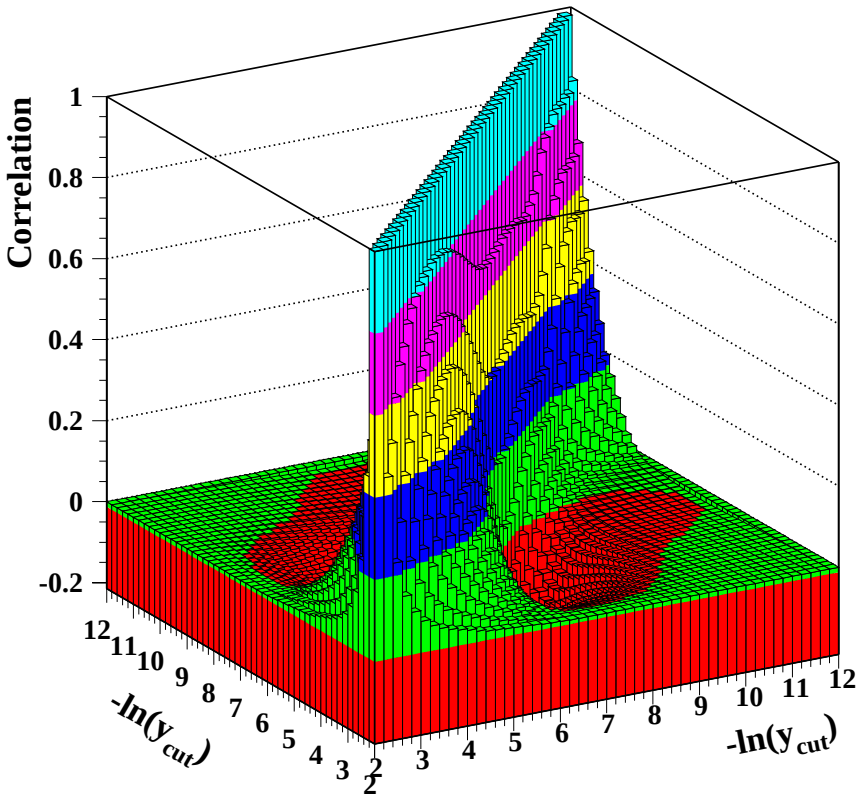

Figure 6.4: Bin-by-bin statistical correlations between measurements of the four-jet rate at different y_{cut} values.

leading to three different measurements of the strong coupling constant.

- **Method I**. The minimization is performed with respect to $\eta = \frac{\alpha_s C_F}{2\pi}$, with x_μ fixed to 1. Later, all the systematic uncertainty estimations will be for $x_\mu = 1$. The scale uncertainty will be estimated as the variation in the fitted η when x_μ is varied in the range $0.5 < x_\mu < 2.$.

- **Method II**. The minimization is performed with respect to η and x_μ. In all the systematic uncertainty estimations both parameters will be fitted again. There is no theoretical uncertainty associated to the scale, as it is a fitted parameter.

- **Method III**. The minimization is first performed with respect to both η and x_μ. The fitted x_μ value is taken as the optimized scale, ${x_\mu}^{\rm opt}$ [1]. Then, all the systematic

[1] Some details and discussion about the optimized scale method can be found in Appendix A

uncertainty estimations are calculated by fitting only η, but with the scale fixed to this optimized value. The scale uncertainty will be estimated by the variation in the fitted η when x_μ is moved in the range $0.5{x_\mu}^{\rm opt} < x_\mu < 2{x_\mu}^{\rm opt}$.

The fit results for the three methods can be found in Tables 6.2 - 6.4, and the plots of the fit results in Figs. 6.5 and 6.6. The new calculations used for this study, which are at NLO for a four-jet observable, are an important ingredient for a future full NNLO prediction for three-jet observables, where a value for x_μ closer to unity might be obtained [24].

$\eta(\mathrm{M_Z})$	x_μ	$\chi^2/N_{\rm dof}$	$\Longrightarrow$	$\alpha_s(\mathrm{M_Z})$
0.02483 ± 0.00003	1.	27.6/5		0.1170 ± 0.0001

Table 6.2: Fit results with statistical errors only for Method I using ALEPH data.

$\eta(\mathrm{M_Z})$	x_μ	$\chi^2/N_{\rm dof}$	$\Longrightarrow$	$\alpha_s(\mathrm{M_Z})$
0.02494 ± 0.00004	0.73 ± 0.05	4.8/4		0.1175 ± 0.0002

Table 6.3: Fit results with statistical errors only for Method II using ALEPH data.

$\eta(\mathrm{M_Z})$	x_μ	$\chi^2/N_{\rm dof}$	$\Longrightarrow$	$\alpha_s(\mathrm{M_Z})$
0.02494 ± 0.00003	0.73	4.8/5		0.1175 ± 0.0001

Table 6.4: Fit results with statistical errors only for Method III using ALEPH data.

A χ^2 per degree of freedom close to unity is found for methods II and III, where a "preferred" value x_μ=0.73 is found. The fitted x_μ in Method II, quite different from unity, might be an indication that missing higher orders in perturbative QCD are still important. This is also reflected in the large χ^2 for Method I, where the scale is not allowed to vary and thus to mimic the contributions from missing higher orders.

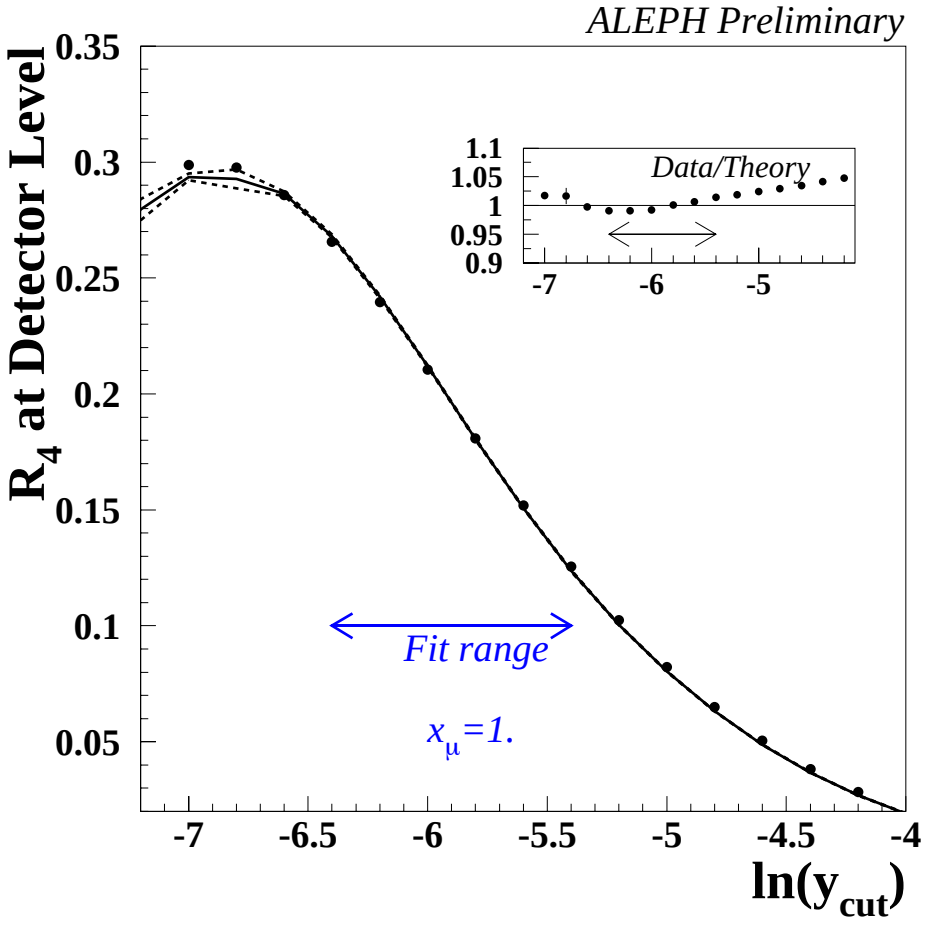

Figure 6.5: Plot for the distribution of the four-jet rate, corrected to detector level and fitted to ALEPH data using Method I. Full dots correspond to ALEPH data and the solid line to the fitted distribution. Dashed lines are also plotted, which correspond to the statistical uncertainty, but they are indistinguishable from the solid line for most of the y_{cut} range. The ratio of data with respect to fitted distributions is shown in the small insert.

Figures 6.5 and 6.5 shows how the fitted four-jet rate significantly deviates from data for low values of $\ln y_{cut}$ out of the fit range. Such deviation is larger when the scale is also fitted, which could be an indication of missing higher orders being more and more important at small y_{cut} values.

Finally, Fig. 6.7 shows the sensitivity of the fit to the renormalization scale, leading to a theoretical uncertainty on η from the scale variation.

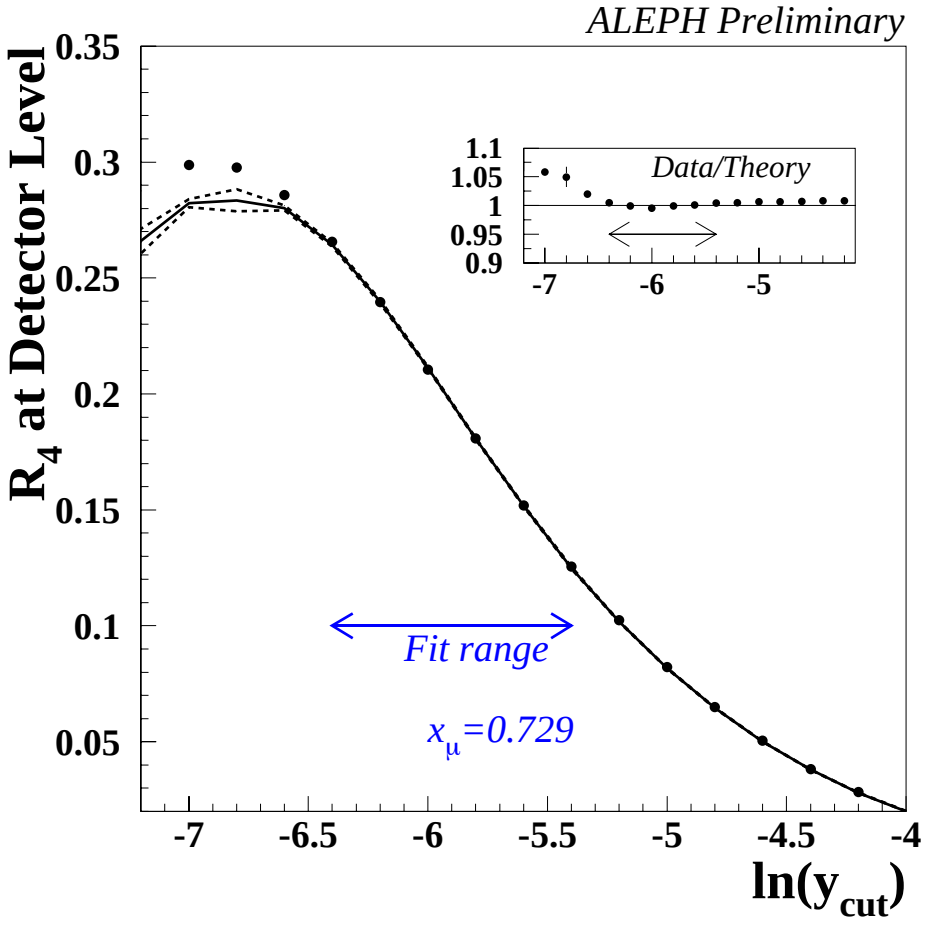

Figure 6.6: Plot for the distribution of the four-jet rate, corrected to detector level and fitted to ALEPH data using Method II. Full dots correspond to ALEPH data and the solid line to the fitted distribution. Again dashed lines are plotted to show the statistical uncertainty, but they are indistinguishable from the solid line for most of the y_{cut} range. The ratio of data with respect to fitted distributions is shown in the small insert.

6.1.3 Systematic Studies

Quedaba mucho por hacer.
Quedaba mucho.
Aprendí a sumar lo lógico y lo incierto.

Tables 6.5-6.7 show the sources of systematic uncertainty that have been studied for the three methods. A brief description of each uncertainty source can be found in the following sections.

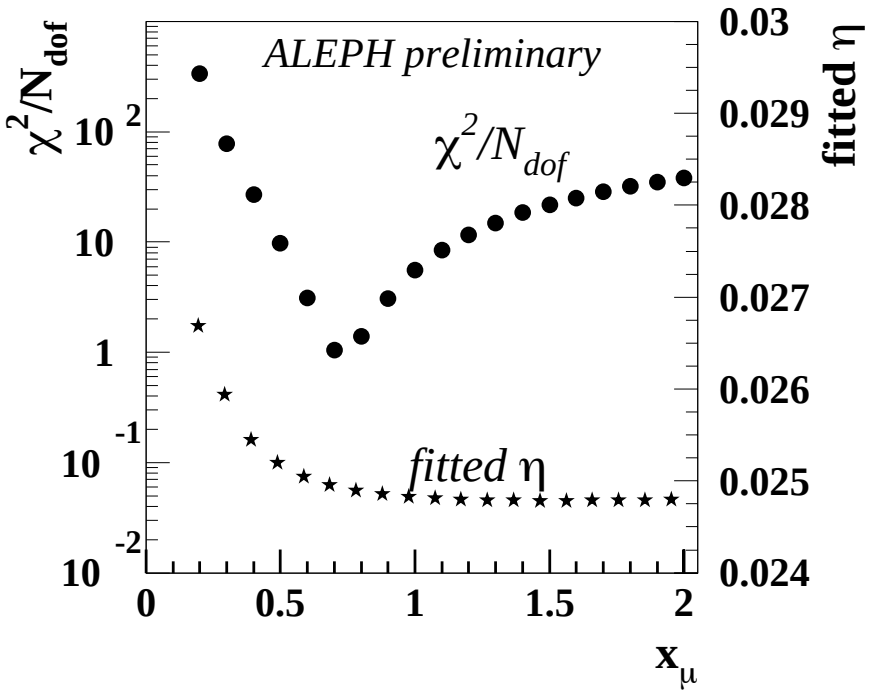

Figure 6.7: Dependence of the fitted η value and the $\chi^2/N_{\rm dof}$ on the renormalization scale x_μ.

Fit Range

The sensitivity of the measurements to the fit range is checked by repeating the analyses with the requirement of a total correction per bin smaller than 20% (it was 10% in the standard analyses). The systematic variation due to this new fit range is quite different for the three methods. For the first method, where x_μ is fixed to 1, the range uncertainty is large with respect to the statistical error. However, for the two other methods this uncertainty is of the same order than the statistical one. This might be an indication of some correlation between the scale and range uncertainties in Method I, which is avoided when x_μ is either fit at the same time as η or fixed to its optimized value.

Selection Criteria

All cuts imposed in the hadronic selection have been varied in order to evaluate the effect on the measurement. The new values for the selection cuts on track parameters are found by changing them until the number of selected events per unit luminosity is the same in data and MC [54]. The analysis has been repeated by introducing the following changes

	$\eta(M_Z)$	χ^2/N_{dof}
tot.corr. $< 20\%$	0.02491 ± 0.00002	57.5/8
Range sys.	$\Delta\eta = 0.00008$	

	$\eta(M_Z)$	χ^2/N_{dof}
HERWIG	0.02461 ± 0.00003	107.3/5
Hadr. Syst.	$\Delta\eta = 0.00006$	

	$\eta(M_Z)$	χ^2/N_{dof}
Charged Only	0.02500 ± 0.00003	33.6/5
Detector sys.	$\Delta\eta = 0.00016$	

	$\eta(M_Z)$	χ^2/N_{dof}
x_μ=0.5	0.02519 ± 0.00003	50.0/5
x_μ=2.	0.02480 ± 0.00002	195.3/5
Scale sys.	$\Delta\eta = 0.00018$	

	$\eta(M_Z)$	χ^2/N_{dof}
Sphericity cut	0.02485 ± 0.00003	29.3/5
TPC cut	0.02480 ± 0.00003	22.2/5
N_{ch} cut	0.02486 ± 0.00003	27.6/5
E_{ch} cut	0.02484 ± 0.00003	28.5/5
θ_{ch} cut	0.02485 ± 0.00003	34.6/5
θ_{nt} cut	0.02479 ± 0.00003	28/2/5
Fraction of e.m. energy cut	0.02483 ± 0.00003	27.1/5
z_0 cut	0.02482 ± 0.00003	28.3/5
d_0 cut	0.02483 ± 0.00003	27.9/5
p_t cut	0.02482 ± 0.00003	26.4/5
Experimental sys.	$\Delta\eta = 0.00013$	

Table 6.5: Systematic uncertainties for Method I.

(only one at a time): at least six measured space coordinates from the TPC; a polar angle at the origin in the range $20° < \theta < 160°$ both for charged and neutral tracks; transverse momentum $p_t > 0.205$ GeV/c; $d_0 = 1.867$cm; $z_0 = 6.64$cm; at least 8 selected charged tracks; minimum charged energy 22 GeV; $|\cos\Theta_{Sph}| < 0.85$; and fraction of electromagnetic energy $< 20\%$.

The observed changes when modifying the selection cuts are in general small and in many cases even negligible, always below 1% for η. These uncertainties are smaller than the equivalent ones obtained with three-jet observables, as might be expected from the quadratic LO dependence on η for four-jet variables instead of the linear one in the case of three-jet variables.

	$\eta(M_Z)$	x_μ	χ^2/N_{dof}	
tot.corr. $< 20\%$	0.02496 ± 0.00003	0.756 ± 0.034	20.3/7	$\rho_{\eta x_\mu}$
Range sys.	$\Delta\eta = 0.00002$	$\Delta x_\mu = 0.027$		1.

	$\eta(M_Z)$	x_μ	χ^2/N_{dof}	
HERWIG	0.02491 ± 0.00005	0.547 ± 0.029	0.7/4	$\rho_{\eta x_\mu}$
Hadr. Syst.	$\Delta\eta = 0.00002$	Δx_μ=0.099		1.

	$\eta(M_Z)$	x_μ	χ^2/N_{dof}	
Charged Only	0.02511 ± 0.00004	0.731 ± 0.046	9.1/4	$\rho_{\eta x_\mu}$
Detector sys.	$\Delta\eta = 0.00009$	$\Delta x_\mu = 0.001$		1.

	$\eta(M_Z)$	x_μ	χ^2/N_{dof}	
Sphericity cut	0.02497 ± 0.00004	0.719 ± 0.047	4.4/4	
TPC cut	0.02489 ± 0.00004	0.750 ± 0.050	4.0/4	
N_{ch} cut	0.02497 ± 0.00004	0.731 ± 0.047	5.1/4	
E_{ch} cut	0.02495 ± 0.00004	0.725 ± 0.047	4.7/4	
θ_{ch} cut	0.02498 ± 0.00004	0.703 ± 0.044	4.9/4	
θ_{nt} cut	0.02490 ± 0.00004	0.728 ± 0.048	5.5/4	
Fraction of e.m. energy cut	0.02494 ± 0.00004	0.732 ± 0.048	4.9/4	
z_0 cut	0.02493 ± 0.00004	0.726 ± 0.047	4.8/4	
d_0 cut	0.02494 ± 0.00004	0.727 ± 0.047	4.8/4	
p_t cut	0.02493 ± 0.00004	0.732 ± 0.048	4.5/4	$\rho_{\eta x_\mu}$
Experimental sys.	$\Delta\eta = 0.00010$	$\Delta x_\mu = 0.039$		-0.741

Table 6.6: Systematic uncertainties for Method II.

The total experimental systematic uncertainty has been computed as the quadratic sum of all contributions, where individual contributions are calculated in the Bayesian approach. It results in an experimental uncertainty on η going from 0.00013 for Method I to 0.00008 for Method III.

Hadronization Corrections

The hadronization correction uncertainty is taken as the Bayesian change in η when the corrections are calculated with HERWIG. This results in a systematic uncertainty much

	$\eta(M_Z)$	χ^2/N_{dof}
tot.corr. $< 20\%$	0.02497 ± 0.00003	20.1/8
Range sys.	$\Delta\eta = 0.00003$	

	$\eta(M_Z)$	χ^2/N_{dof}
HERWIG	0.02473 ± 0.00003	27.9/5
Hadr. Syst.	$\Delta\eta = 0.00004$	

	$\eta(M_Z)$	χ^2/N_{dof}
Charged Only	0.02511 ± 0.00003	9.1/5
Detector sys.	$\Delta\eta = 0.00008$	

	$\eta(M_Z)$	χ^2/N_{dof}
x_μ=0.365	0.02559 ± 0.00004	193.3/5
x_μ=1.458	0.02479 ± 0.00003	101.8/5
Scale sys.	$\Delta\eta = 0.00005$	

	$\eta(M_Z)$	χ^2/N_{dof}
Sphericity cut	0.02496 ± 0.00003	4.4/5
TPC cut	0.02490 ± 0.00003	4.2/5
N_{ch} cut	0.02497 ± 0.00003	5.1/5
E_{ch} cut	0.02494 ± 0.00003	4.7/5
θ_{ch} cut	0.02496 ± 0.00003	5.2/5
θ_{nt} cut	0.02490 ± 0.00003	5.5/5
Fraction of e.m. energy cut	0.02494 ± 0.00003	4.9/5
z_0 cut	0.02490 ± 0.00003	5.5/5
d_0 cut	0.02494 ± 0.00003	4.8/5
p_t cut	0.02493 ± 0.00003	4.6/6
Experimental sys.	$\Delta\eta = 0.00008$	

Table 6.7: Systematic uncertainties for Method III.

smaller than 1% for the three methods. In methods I and III, the χ^2 of the fit when using HERWIG corrections is almost four times the one of the standard measurement. Therefore, the uncertainty calculated using the Bayesian method is heavily reduced if compared to the full difference between the fit results of measurements using PYTHIA and HERWIG corrections. However, even if the full difference is taken as an estimate of the hadronization uncertainty, it would be small (0.00022), not even reaching the 1% range.

Detector Corrections

An estimation of the systematic uncertainty due to the detector corrections has been obtained by repeating the analysis using charged tracks only, leading to a variation in η

going from 0.6% to 0.3%, depending on the method.

Theoretical Predictions

The lack of knowledge of higher orders of perturbative QCD is estimated by the impact on η of the renormalization scale variation for Methods I and III. In the second Method there is no uncertainty related to the scale as it is fitted for each variation of the analysis.

The scale uncertainty is the largest contribution to the total systematic uncertainty in the case of Method I as can be seen in Table 6.5. For Method III, this uncertainty is heavily reduced to less than 1/3 of its value in the first case. This is a well known feature of the optimized scale method as is further explained in Appendix A.

6.1.4 Further Checks

Hadronization Corrections

As a cross-check, the more extreme models presented in Sect. 5.3.1 were used to fit η. The systematic changes in the fitted parameters, see Table 6.8, are covered by the total uncertainty as will be seen in Section 6.1.5.

	$\eta(\mathrm{M_Z})$	x_μ	χ^2/N_{dof}
PYTHIA ME - Method I	0.02569 ± 0.00003	1.	80.6/5
PYTHIA ME - Method II	0.02589 ± 0.00005	0.637 ± 0.030	3.4/4
PYTHIA ME - Method III	0.02581 ± 0.00003	0.729	11.3/5
PYTHIA,Q_0 - Method I	0.02527 ± 0.00003	1.	178.5/5
PYTHIA,Q_0 - Method II	0.02563 ± 0.00005	0.526 ± 0.023	11.3/4
PYTHIA,Q_0 - Method III	0.02539 ± 0.00003	0.729	60.7/5

Table 6.8: Check for the hadronization corrections. The deviations from the standard analysis are covered by the systematic uncertainties already described.

Scale Dependence when using PYTHIA or HERWIG

In the results for Method III, the fitted scale was found to be quite different when using the hadronization corrections coming from PYTHIA (0.73) or HERWIG (0.55). The check described in this section was carried out in order to understand the source of this

effect. The fit was repeated, for some arbitrarily chosen ranges, both using corrections from PYTHIA and HERWIG. The results can be found in Table 6.9. The discrepancies in the fitted x_μ are found to be larger when going to small values of $\ln(y_{cut})$, where the PYTHIA and HERWIG corrections differ more from each other, see Fig. 6.1. In fact, the first two entries of the table show quite close x_μ values for PYTHIA and HERWIG (compatible within errors), as they correspond to the ranges with very similar corrections. Therefore, the different fitted x_μs obtained in the fits when using PYTHIA and HERWIG corrections are just a propagation of the discrepancies of the hadronization corrections themselves and are then covered by the hadronization + range uncertainties. In any case, the variations in the fitted η, within one type of corrections, are small (especially for the PYTHIA case).

	PYTHIA		HERWIG	
Range	$\eta(M_Z)$	x_μ	$\eta(M_Z)$	x_μ
$-6. \to -4.2$	0.02497	0.66	0.02483	0.61
$-6. \to -5.$	0.02499	0.64	0.02485	0.59
$-6.2 \to -5.2$	0.02498	0.67	0.02488	0.57
$-6.4 \to -5.4$	0.02494	0.73	0.02491	0.55
$-6.6 \to -5.6$	0.02489	0.83	0.02487	0.58
$-6.8 \to -5.8$	0.02496	0.75	0.02485	0.59

Table 6.9: Check for the difference in the optimized scale when using PYTHIA or HERWIG to correct for hadronization effects.

Fits over different ranges of R_4

There is an ongoing discussion with the DELPHI experiment about the meaning of fitting the four-jet rate with x_μ fixed to 1 [56]. The DELPHI Collaboration uses as standard measurement the optimized scale method (i.e. Method III in this analysis) but with the theoretical prediction only at NLO. Such a decision was taken after performing the following test. Small ranges of R_4 at different values of $\ln(y_{cut})$ were fitted to DELPHI data, using resummed predictions, and significantly different η values were found. Such variations in the fitted η brought them to the conclusion that missing higher order terms were important and that the scale should be fitted at the same time. However, they claim that it has no physical meaning to fit the scale when a resummed prediction is used. We have also studied such variations but different conclusions were extracted.

The check is the following. The resummed four-jet rate was fitted at different small ranges covering in total a large region in terms of $\ln(y_{cut})$. The method used for the fit was always Method I. Results can be found in Table 6.10, where $\Delta\eta_{range}$ is calculated as the largest difference between the measurement at a given range and any of the measurements at other ranges. Then, the fit was repeated for the same ranges, but now with x_μ first fixed to 0.5 and then to 2, i.e. the scale uncertainty for each range was obtained. Results for the scale uncertainty estimation are found in Table 6.11. A large correlation between the range uncertainty and the scale uncertainty is observed, which implies that the "bias" in the fitted η which could be introduced by selecting a given range is fully covered by the scale uncertainty in each case, i.e. the fitted η values together with their scale uncertainty for the different ranges are fully compatible.

Range	$\eta(M_Z)$	$\Delta\eta_{range}$
$-5. \to -4.$	0.02511	0.00028
$-5.2 \to -4.2$	0.02508	0.00025
$-5.4 \to -4.4$	0.02506	0.00023
$-5.6 \to -4.6$	0.02501	0.00018
$-5.8 \to -4.8$	0.02497	0.00014
$-6. \to -5.$	0.02492	0.00019
$-6.2 \to -5.2$	0.02488	0.00023
$-6.4 \to -5.4$	0.02483	0.00028

Table 6.10: Variation in the the fitted η when using different ranges for the resummed four-jet rate.

Range	η for x_μ=0.5	η for x_μ=2.	$\Delta\eta_{scale}$
$-5. \to -4.$	0.02494	0.02547	0.00036
$-5.2 \to -4.2.$	0.02497	0.02538	0.00030
$-5.4 \to -4.4$	0.02498	0.02533	0.00027
$-5.6 \to -4.6$	0.02503	0.02520	0.00019
$-5.8 \to -4.8$	0.02506	0.02511	0.00014
$-6. \to -5.$	0.02509	0.02500	0.00017
$-6.2 \to -5.2$	0.02513	0.02491	0.00025
$-6.4 \to -5.4$	0.02520	0.02480	0.00037

Table 6.11: Estimation of the scale uncertainty for different ranges of the four-jet rate.

Another estimation of the scale uncertainty for Method III

If the χ^2 obtained for the experimentally optimized scale method is taken at face value and if this method is used for the standard fit, then the scale uncertainty can be computed as the change in the fitted η when x_μ is fixed to a value ${x_\mu}^{\rm new}$ such that $\chi^2({x_\mu}^{\rm new}) = \chi^2({x_\mu}^{\rm opt}) + 1$. For the fit presented in Section 6.1.2 the optimized scale value was 0.73, and a variation of one in the χ^2 corresponds to the x_μ values of 0.69 and 0.78. The fit results are found in Table 6.12, which give a scale uncertainty of 0.00003 to be compared to 0.00005 obtained with the estimation used in Section 6.1.3.

η	x_μ	$\chi^2/N_{\rm dof}$
0.02497 ± 0.00003	0.69	5.9/4
0.02491 ± 0.00003	0.78	5.9/4

Table 6.12: Estimation of the scale uncertainty for Method III using as criteria a variation of 1 in the χ^2.

Effect of the K coefficient in the resummed prediction

It was stated in Chapter 3 that if the K coefficient was taken into account in the splitting probabilities, an improved theoretical prediction could be obtained. This had been observed for the two-jet rate [26], but it is also true for the four-jet rate as seen in Fig. 6.8. In the figure the improved resummed prediction is shown to better reproduce the ALEPH data. Thus, the resummed prediction without this K coefficient was not taken into account for the measurements of this thesis.

6.1.5 Final Results

Putting together all systematic uncertainties considered above, the final results of the measurements of the strong coupling constant are:

$$\eta(\mathrm{M_Z}) = 0.02483 \pm 0.00003(stat) \pm 0.00029(sys)$$
$$\Downarrow$$
$$\alpha_s(\mathrm{M_Z}) = 0.1170 \pm 0.0001(stat) \pm 0.0014(sys)$$

for Method I,

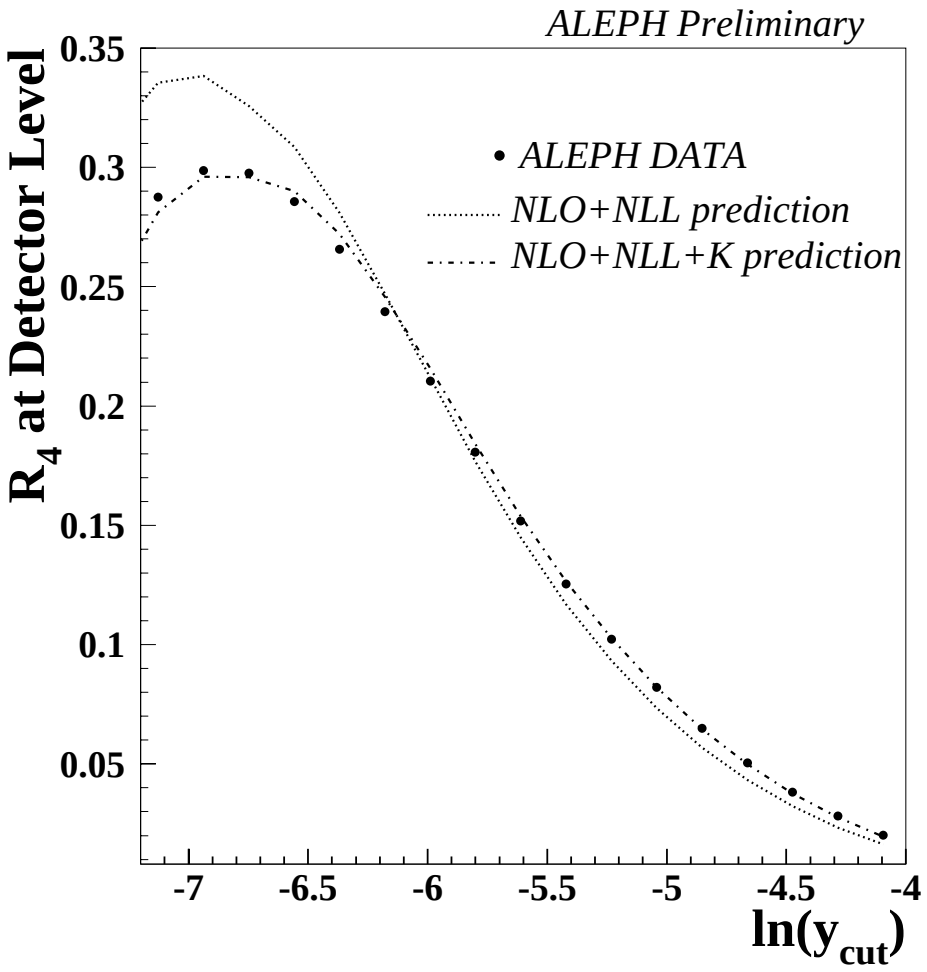

Figure 6.8: Comparison of the four-jet rate as obtained from ALEPH data to the resummed predictions, with and without the K coefficient, from DEBRECEN.

$$\eta(\mathrm{M_Z}) = 0.02494 \pm 0.00004(stat) \pm 0.00013(sys)$$
$$x_\mu = 0.73 \pm 0.05$$
$$\Downarrow$$
$$\alpha_s(\mathrm{M_Z}) = 0.1175 \pm 0.0002(stat) \pm 0.0006(sys)$$

for Method II and, finally for Method III,

$$\eta(\mathrm{M_Z}) = 0.02494 \pm 0.00003(stat) \pm 0.00014(sys)$$
$$\Downarrow$$
$$\alpha_s(\mathrm{M_Z}) = 0.1175 \pm 0.0001(stat) \pm 0.0007(sys) \quad .$$

If the Bayesian method had not been used, and all the contributions for each uncertainty source had been added quadratically instead, the total systematic error in α_s would be of 0.0022, 0.0008 and 0.0033, respectively.

The results presented above are in good agreement with previous measurements by ALEPH using two- and three-jet observables [54], but the dominant source of uncertainty, the theoretical uncertainty, is strongly reduced when using the four-jet rate. Such results are confirmed by a preliminary analysis from the DELPHI collaboration, which also uses the four-jet rate [56]. These results are one of the most precise determinations on α_s at present.

6.2 A Simultaneous Measurement of the Strong Coupling Constant and the Colour Factors

Tests of the structure of the underlying gauge group [21][55], which is $SU(3)$ in the case of QCD, have been performed at LEP. In order to get sensitivity to the gauge structure of the theory, the angular distributions of jets in four-jet events were employed. The first tests of the structure of the underlying gauge group were done using LO predictions which start at $\mathcal{O}(\alpha_s^2)$ [57].

Leading order calculations in pQCD give only the order of magnitude of a partonic cross section and the main features of the distribution of a certain observable. This poor predictivity of the theory is usually signalled by a strong dependence of the (unphysical) renormalization and factorization scales. The theoretical accuracy of pQCD predictions is in general controlled by higher (at least NLO) order corrections that reduce the scale sensitivity.

In this section a new combined measurement of the strong coupling constant and the colour factors using NLO calculations is presented, by fitting the resummed next-to-leading order predictions for the four-jet rate and the normalized next-to-leading order predictions for the angular correlations of the four-jet events to corrected ALEPH data. A new treatment of the backgrounds and hadronization corrections is used, showing good agreement with previous results. In the following subsections details about corrections, fit results and systematic uncertainties are given. Recently, first results on a combined measurement of the strong coupling constant and the colour factors, which are based on NLO calculations, have been published by OPAL [55].